Applied Surface Science 540 (2021) 148103

Contents lists available at ScienceDirect

Applied Surface Science

journal homepage: www.elsevier.com/locate/apsusc

Ion irradiation induced surface composition modulation in equiatomic binary alloys

Byung-Hyun Kim [a,b,c,*], Sang-Pil Kim [b,d,1], Joonhee Kang [a], Yong-Chae Chung [c], Kyung-Suk Kim [d], Kwang-Ryeol Lee [b,*]

[a] Platform Technology Laboratory, Korea Institute of Energy Research, Daejeon 34129, Republic of Korea
[b] Computational Science Research Center, Korea Institute of Science and Technology, Seoul 02792, Republic of Korea
[c] Division of Materials Science and Engineering, Hanyang University, Seoul 04763, Republic of Korea
[d] School of Engineering, Brown University, Providence, 02912 RI, USA

ARTICLE INFO

Keywords:
Ion irradiation
Ion bombardment
Sputtering
Equiatomic alloys
Molecular dynamics

ABSTRACT

Composition modulation by Ar bombardment on the $Co_{0.5}Cu_{0.5}$ alloy and the CoAl B2 phase was investigated on atomic scale by molecular dynamics simulation. The Ar bombardment on alloys at 300 K revealed that this bombardment induces a surface composition modulation in the layer-by-layer mode. In both the $Co_{0.5}Cu_{0.5}$ alloy and the CoAl B2 phase, the element of higher-sputtering yield is accumulated on the top surface layer, whereas it is depleted in lower layers, which is puzzling in the framework the conventional sputtering theory. A phenomenological kinetic model derived from the MD simulation results considering both the rearrangement and the sputtering of the substrate atoms successfully demonstrated that the rearrangement of the substrate atoms plays a significant role in the observed composition modulation.

1. Introduction

Ion irradiation on materials draws much attention due to not only fundamental interests but also its impact on various technological issues such as semiconductor processing and developing structural materials with outstanding irradiation resistance [1–9]. A recent theoretical study on a Si/SiO_2 heterostructure interface for low-power single-electron transistors revealed that ion irradiation with high fluences can cause ion mixing at the interface leading to coordination defects which eventually affect the device performance [5]. Granberg et al. studied about a reduction of damage accumulation induced by ion bombardment in equiatomic multicomponent alloys and revealed that these alloys are resistance to radiation damage due to a significant reduction of dislocation mobility [9]. Understanding of materials' mechanical, physical and chemical properties under or after ion irradiation, thus, is of great interest.

Self-organized nanostructures of dots, holes or ripples produced by energetic ion bombardment have been reported in a wide variety of substrates [10–18]. Ion bombardment on an alloy or a compound becomes even more interesting since it can induce a surface composition modulation with a topographical surface structure evolution [19–21], which is, however, hardly explained by the classical kinetic model. Extensive theoretical studied have tried to elucidate many of the pertinent processes resulting in the composition changes in multicomponent materials during sputtering [21,20,22]. The models considered both *primary* and *secondary* processes which was supposed by Sigmund [23–29]: the former is associated with the species-dependent sputtering rate (preferential sputtering) and the latter with further changes of the target composition due to effects initiated by the ion irradiation such as collisional mixing, radiation-induced diffusion or segregation, Gibbsian segregation or ion implantation [22,30]. The *primary* process which is governed by the binding energy and atomic mass was studied by ion bombardment of isotopic mixtures [30]. However, it is usually impossible to assess the contribution of individual processes to composition changes unambiguously, because the processes simultaneously occur and frequently interfere with themselves. In addition, several of physical and chemical properties of the species relevant to the processes are not known very well.

* Corresponding authors at: Platform Technology Laboratory, Korea Institute of Energy Research, Daejeon 34129, Republic of Korea (B.-H. Kim) and Computational Science Research Center, Korea Institute of Science and Technology, Seoul 02792, Republic of Korea (K.-R. Lee).
E-mail addresses: bhkim@kier.re.kr (B.-H. Kim), krlee@kist.re.kr (K.-R. Lee).
[1] Current address: R&D Center, Samsung SDI CO., LTD., Suwon 16678, Republic of Korea.

https://doi.org/10.1016/j.apsusc.2020.148103
Received 14 September 2020; Received in revised form 5 October 2020; Accepted 5 October 2020
Available online 16 October 2020

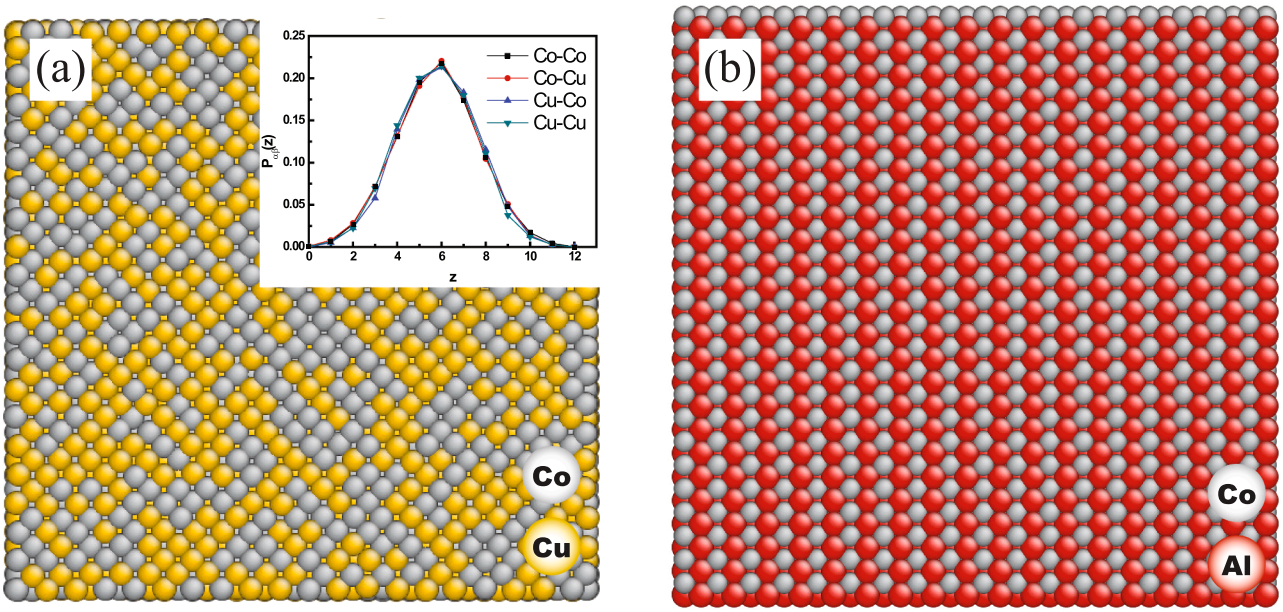

Fig. 1. Top view of the (001) surface of the $Co_{0.5}Cu_{0.5}$ alloy substrate (a) and the (011) surface of CoAl ordered B2 phase.

As a pioneering study on ion irradiation of a binary compound, Shenoy et al. extended the classical model of the sputter-induced surface structure evolution of a pure system to a model of the sputtering phenomena on an alloy surface [19]. They showed that the preferential sputtering and the difference in diffusivities of alloy components could lead to spontaneous modulations in surface composition along with the formation of periodic ripple patterns on the surface. Their results suggested a simple method to simultaneously achieve nanoscale patterning of both surface morphology and composition. In a series of papers, Bradley and his co-workers also extended the ion irradiation model by including concurrent deposition of impurities or a functional form for surface composition dependent sputtering yields to explain the surface composition changes due to ion irradiation on alloys [20,21] However, the rearrangement of the substrate atoms due to ion irradiation, which might play a great role in composition changes of alloys, was not considered or considered in a limited way in these theoretical works.

On the other hand, the molecular dynamics (MD) simulations have been widely used to study the sputtering phenomena by directly tracing the motion of atoms [31]. For example, MD simulations of ionic bombardment on the surfaces of Si, Au, Pd or SiO_2 have revealed the significance of surface-layer atomic rearrangement resulting in the formation of large craters at the point of impact with a heap of atoms nearby [32–35]. Thus MD simulation of the ion bombardment can be utilized as a suitable method to provide the details of the atomic transport on the surface. By statistically counting the number of sputtered and rearranged atoms after the simulation, it is possible to derive the parameters that represent the net effects of the *primary* and *secondary* processes.

In the present work, we performed the MD simulations as a tool to derive a new kinetic model, which directly uses the motion of atoms that evolve by ion irradiation, instead of using the Sigmund sputtering theory or its extensions. Based on the MD simulations, we derived a phenomenological kinetic model which also can be directly compared with the simulation results to understand the surface phenomena during ion bombardment. The present MD simulation revealed that a layer-by-layer composition modulation occurred by the Ar bombardment on both $Co_{0.5}Cu_{0.5}$ and CoAl surfaces. A phenomenological model that considers both the rearrangement and the sputtering is in good agreement with the simulation results, which indicates that the rearrangement should be properly considered along with the preferential sputtering. We hope that our results provide an important insight to understand the evolution of surface structure and composition during ion irradiation on alloys.

2. Computational methods

We carried out MD simulations of Ar bombardments on two binary systems of contrasting thermodynamic properties: a Co-Cu system and a Co-Al system. The Co-Cu system is almost immiscible at 300 K while the Co-Al system has a stable CoAl-intermetallic phase of a B2-type structure. The $Co_{0.5}Cu_{0.5}$ alloys were made by randomly distributing Co and Cu on the *fcc* lattice points at the same atomic fraction. Fig. 1(a) is an example of the (001) surface of the $Co_{0.5}Cu_{0.5}$ alloy. Inset of the Fig. 1(a) shows the partial probability function $P_{\alpha\beta}(z)$ of which an α atom has z neighbors of β atoms in its first-nearest neighbor shell. For all atomic parings, they are essentially identical with a maximum at $z = 6$, which is typical of random *fcc* alloys. Fig. 1(b) shows the (011) surface of CoAl B2 phase built from a well-known ordered B2 structure. The size of the $Co_{0.5}Cu_{0.5}$ alloy substrate was $7.23 \times 7.23 \times 3.62$ nm^3 with (001) surface, while that of CoAl B2 phase was $7.28 \times 7.15 \times 4.28$ nm^3 with (011) surface. Periodic boundary conditions were adopted in the horizontal directions. The atomic positions of the bottom two layers were fixed to simulate a thick substrate. The temperature of the bottom half of the remaining layer was kept at 300 K to play a role of thermal bath during Ar bombardments. All the other atoms were unconstrained. The alloys were relaxed for 50 ps before starting Ar bombardments.

Neutral Ar atoms of kinetic energy 0.5 keV were then bombarded at 300 K in the direction normal to the surface. The simulation temperature and the kinetic energy of Ar were chosen to mimic typical sputtering experiments using a broad ion beam source, where the ion energy ranges from 0.1 to 1 keV [10,11]. The positions of the Ar incidence were

Table 1
Summary of the benchmark test for the potentials used in this study (Co, Cu).

Property	Co		Cu	
	Exp. or DFT	Calc.	Exp. or DFT	Calc.
a_0 (Å)	3.55 [36]	3.555	3.61 [37]	3.614
E_{coh} (eV)	4.38 [36]	4.45	3.49 [37]	3.54
B (GPa)	191.4 [37]	175.1	137 [37]	133.8
γ_{111} (mJ/m^2)	2700 [38]	1954	–	1504
γ_{100} (mJ/m^2)	2780 [38]	2100	1600 [39]	1568
γ_{110} (mJ/m^2)	–	2294	–	1757

Table 2
Summary of the benchmark test for the potentials used in this study (Co, Al).

Property	Co		CoAl		Al	
	Exp. or DFT	Calc.	Exp. or DFT	Calc.	Exp. or DFT	Calc.
a_0 (Å)	3.55 [36]	3.54	2.86 [40]	2.86	4.05 [41]	4.05
E_{coh} (eV)	4.38 [36]	4.38	4.47 [42]	4.47	3.36 [41]	3.37
B (GPa)	191.4 [37]	193.8	161 [43]	174	72.2 [37]	79.6
γ_{111} (mJ/m^2)	2700 [38]	1000	–	1863	935 [44]	831
γ_{100} (mJ/m^2)	2780 [38]	1196	-	1799	1081 [44]	869
γ_{110} (mJ/m^2)	–	1364	–	1574	1090 [44]	1006

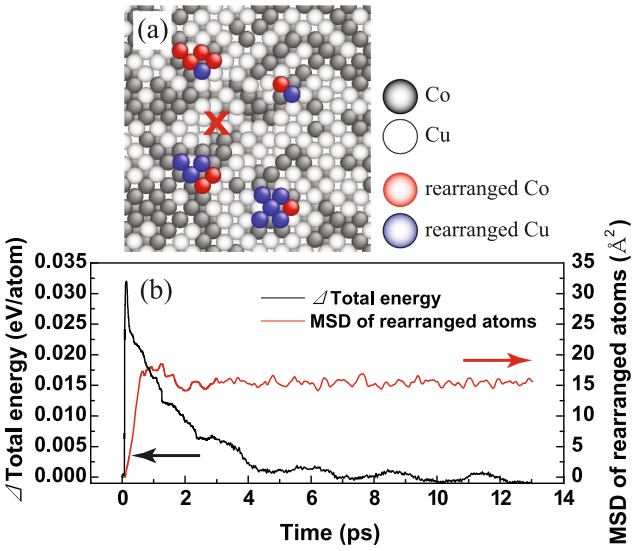

Fig. 2. (a) Atomic configuration of $Co_{0.5}Cu_{0.5}$ alloy surface after 0.5 keV Ar bombardment. (b) The total energy change of the system and mean square displacement of the rearranged atoms during the simulation.

randomly selected. Since the Ar bombardment can reduce the distance between atoms, a strong repulsive force between atoms should be considered in the present simulation. We combined the embedded atom method (EAM) potential [45–48] with the Ziegler, Biersack and Littmark (ZBL) potential [49] using a switching function for the potential between metallic elements (see the supplementary information). The interaction of Ar-metals or Ar-Ar pair was expressed by the universal ZBL potential [49]. The EAM potentials used in this study were rigorously benchmarked by using the calculated or experimentally observed lattice constants, mechanical properties, surface energies and the cohesive energy of the elements. Table 1 and 2 summarize the benchmark test of the potentials used for Co-Cu system and for Co-Al system, respectively. Lattice constants, cohesive energy and elastic constants exhibit quantitative consistency between molecular static calculations and experiments or the first-principles density functional theory (DFT) calculations. The qualitative relationship between the surfaces is in good agreement with the DFT calculations. For example, the calculated surface energy of Co is larger than those of Cu and Al, as in the DFT calculations, although the surface energy of Co is underestimated for all orientations. Orientation dependence of the surface energy is well described by these potentials.

Table 3
Normalized sputtering and rearrangement yields in $Co_{0.5}Cu_{0.5}$ alloy and CoAl B2 phase.

$Co_{0.5}Cu_{0.5}$ Alloy				CoAl B2 Phase			
Y^s_{Co}	Y^s_{Cu}	Y^r_{Co}	Y^r_{Cu}	Y^s_{Co}	Y^s_{Al}	Y^r_{Co}	Y^r_{Al}
2.10	2.60	1.00	4.81	1.13	1.78	8.55	14.94

The time step was 0.1 fs for the first 3 ps and 1.0 fs for the next 20 ps. The time interval between two consecutive bombardments on the substrate was fixed at 23.0 ps. Three sets of 2,000 Ar bombardment simulations were carried out to reduce statistical errors. After 2,000 Ar bombardments, about 4.5 and 3.0 atomic layers were eroded in $Co_{0.5}Cu_{0.5}$ and CoAl B2 phase surface, respectively. "Large-scale Atomic/Molecular Massively Parallelized Simulator" (LAMMPS) code was used for all the simulations [50].

3. Results and discussion

Fig. 2(a) shows the atomic configuration of $Co_{0.5}Cu_{0.5}$(001) surface after an energetic Ar bombardment hit the surface at the position marked by **X**. Gray and white balls represent Co and Cu atoms of the substrate, respectively. Red and blue balls are respectively the rearranged Co and Cu atoms placed above the original surface after the Ar bombardment. As the energetic Ar transfers its kinetic energy to the substrate, a thermal spike followed by a micro-explosion and rapid relaxation of the surface atoms occurs, resulting in both sputtering and rearrangement of the surface atoms [51]. Fig. 2(b) shows total energy change of the system and mean square displacement (MSD) of the rearranged atoms during an Ar bombardment. The total energy of the system rapidly increased by the Ar bombardment as the kinetic energy of Ar is transferred to the substrate atoms. However, most of the increased energy dissipated in about 4 ps after the bombardment. MSD data shows that the atomic movement occurs within 1 or 2 ps after the Ar bombardment. It is thus inferred that the surface reaction is ballistic and finishes within at most 4 ps after the Ar bombardment. Thermally-activated surface diffusion was not to be expected once the

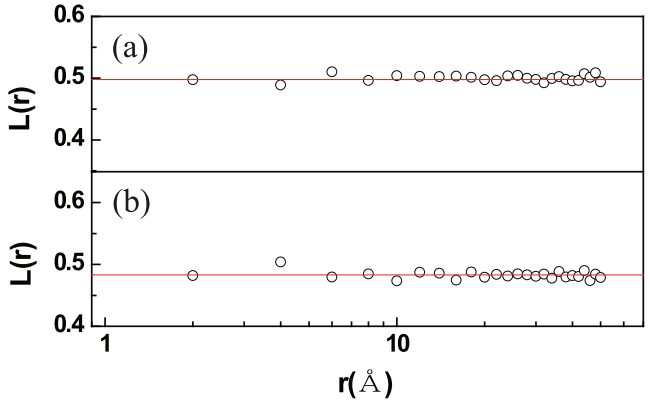

Fig. 3. The composition-composition correlation functions after 2,000 Ar bombardments on the surface of (a) $Co_{0.5}Cu_{0.5}$ alloy and (b) CoAl B2 phase.

bombarded surface was cooled to 300 K. The same behavior was observed on the CoAl(011) surface except that surface amorphization occurs. The surface amorphization would result from the high cohesive energy of the Co-Al bond, which enacts a higher energy barrier to the ballistic relaxation.

We calculated the average sputtering yield and the rearrangement yield of each atom using 1,000 independent Ar bombardment simulations. The normalization of the yield was made by dividing the number of sputtered or rearranged atoms by the composition of the element. The bombardment position of Ar was randomly selected within a surface unit cell for each bombardment event. *Sputtered atoms* are defined to be those that are removed from the surface, while *rearranged atoms* are those that are located above the original surface after 23 ps from the Ar bombardment. Table 3 summarizes the calculated results of the normalized alloy sputtering yield (Y^s_α) and rearrangement yield (Y^r_α) of element α. In the $Co_{0.5}Cu_{0.5}$ alloys, Y^r_{Cu} is 1.85 times larger than its sputtering yield, Y^s_{Cu}. In contrast, Y^r_{Co} is smaller than its sputtering yield, Y^s_{Co}. Comparing the two, both the sputtering and rearrangement yields of Cu are higher than those of Co. In the case of CoAl in its B2 phase, both Co and Al have higher rearrangement yields than their sputtering yields (7.57 times in Co and 8.39 times in Al). Al has higher values of both sputtering and rearrangement yields when compared to Co. The different response of the elements to the Ar bombardment would affect composition modulation during ion bombardment. The composition modulation of the surface was characterized during 2,000 consecutive bombardments of Ar on the alloys (estimated fluence is about $3.8 \times 10^{15}/cm^2$). First, we investigated the lateral composition modulation. The composition-composition correlation function $L_\alpha(r)$ of element α of the surface was evaluated by defining it as the average value of $[\zeta_\alpha(r) - \zeta_\alpha(O)]^2$ over all the reference point on the surface:

$$L_\alpha(r) = \langle [\zeta_\alpha(r) - \zeta_\alpha(O)]^2 \rangle \quad (1)$$

where $\zeta_\alpha(O)$ is the composition of α at any chosen reference point O and $\zeta_\alpha(r)$ is the composition of α at a distance r away from O. (In the atomic scale analysis, $\zeta_\alpha(r)$ may have a value of 0 or 1.) By definition, $L_\alpha(r)$ has the value twice of the difference between the mean square and the autocorrelation values of the surface composition fluctuation (see the supplementary information). Fig. 3(a) and 3(b) show $L_\alpha(r)$ for Cu and Al after 2,000 Ar atoms bombarded the surface of the $Co_{0.5}Cu_{0.5}$ alloy and the CoAl B2 phase, respectively. In both cases, $L_\alpha(r)$ for each material has a constant value irrespective to the distance r. Solid lines in Fig. 3 are corresponding to that of the twice of the mean square of the surface

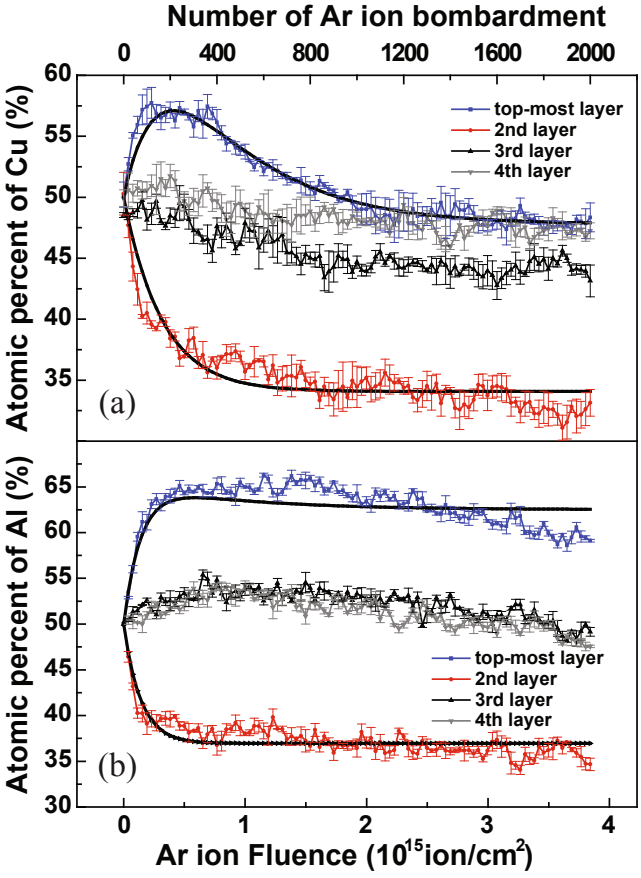

Fig. 4. The composition variation of each atomic layer during the Ar bombardments on (a) the $Co_{0.5}Cu_{0.5}$ alloy and (b) the CoAl B2 phase.

composition fluctuation. This result shows that the lateral surface composition is not correlated in any scale at this ion fluence.

On the contrary, we observed the layer-by-layer composition modulation, which was induced by the Ar bombardment. Fig. 4(a) and 4(b) show the composition variation of each atomic layer during the Ar bombardment on the $Co_{0.5}Cu_{0.5}$ alloy and the CoAl B2 phase, respectively. Atomic layer at a set Ar fluence was defined from the atomic configurations generated by the repeated Ar bombardment of that fluence. In the $Co_{0.5}Cu_{0.5}$ alloy, Cu concentration in the top layer increased in the early stage of sputtering while that in the second layer decreased. As the Ar bombardment proceeded, the concentration of Cu in the second layer continued to decrease to a saturated concentration level ($33 \pm 1\%$) that is considerably smaller than the initial concentration. In the top layer, the Cu concentration shows a maximum of $57 \pm 1\%$ at the fluence of about $0.5 \times 10^{15}/cm^2$. This concentration gradually decreased to its initial levels as the Ar bombardment proceeded. Composition variations in the lower layers are not as significant as in the top two layers. Similar behavior was observed in the CoAl B2 phase surface (see Fig. 4(b)). On the amorphous CoAl surface, the top most layer atom was defined as that has less than 4 neighbor atoms in the first neighbor distance above the atom's position. Atoms in the second layer were then defined by the same criteria after the top layer atoms were removed from the system. Al concentration of the top layer rapidly increased to $65 \pm 1\%$ during the Ar bombardment and slowly decreased after the Ar reached a fluence of $1.5 \times 10^{15}/cm^2$, while that in the second layer monotonically decreased to $36 \pm 1\%$. V. Blum et al. reported that about 20% of the second layer Al atoms are substituted by Co, i.e., Co is enriched in the second layer, which partially agrees with our simulation result [52].

In spite of considerable difference in the thermodynamic properties of the two binary systems, the layer-by-layer composition modulation is commonly observed. It must be further noted that the atoms of higher-sputtering yield, Cu or Al in the present cases (see Table 3), accumulate on the top layer. This result is puzzling in the framework of the Bradley-Harper linear instability theory, which is essentially based on the negative deposition concept. However, these observations would be understood when the rearrangement of surface atoms is considered: atoms with higher rearrangement yield would preferentially move to the top layer during Ar bombardments. The rearrangement should result from the *secondary* processes of the collisional mixing, the radiation-enhanced diffusion and the Gibbsian segregation as discussed in the previous theoretical analysis of high temperature alloy sputtering [25–29]. The *secondary* processes can be significant even at the room temperature since the high temperature spike of the cascade will provide a kinetic environment appropriate for the considerable atomic transport by the ballistic rearrangement. Therefore, the sputtering and rearrangement yields in Table 3 would respectively represent the net effects of the species-dependent *primary* processes and the radiation-induced *secondary* processes. As the atoms accumulated onto the top layer, the sputter erosion from this top layer increases while the rearrangement to the top layer decreases due to the decreased concentration in the lower layer. These two processes of sputtering and rearrangement govern the initial transient behavior of the composition modulation. In the steady state, the rearrangement and the sputtering would be so balanced that the composition of each layer becomes invariant with respect to the ion fluence.

We compared the MD simulation results with a simplified phenomenological kinetic model considering both sputtering and rearrangement. As observed in the MD simulations described above (see Fig. 4), the concentration distribution $\mathbf{C}^{\alpha}\left(=\left\{C_i^{\alpha}; i=1,\cdots,N\right\}\right)$ of the α atom evolves with respect to fluence I, within N layers of atoms which comprise the rearrangement range of α atoms caused by the ion irradiation. At any instant of time (or fluence), the top most surface atomic layer is denoted as the first layer, and higher numbers of atomic layers are assigned with respect to the first layer. As the ion irradiation erodes the alloy sample, the atomic layers are continuously re-numbered. For such process, the evolution of the concentration distribution can be described by

$$\frac{dC_i^{\alpha}}{dI} = F_i^{\alpha}\left(\mathbf{C}^{\alpha}; \boldsymbol{\kappa}^I, C^{\alpha_0}\right), i = 1, \cdots, N \tag{2}$$

which states that the concentration change rate of the ith layer is a function, $F_i^{\alpha}\left(\mathbf{C}^{\alpha}; \boldsymbol{\kappa}^I, C^{\alpha_0}\right)$, of the concentration distribution $\mathbf{C}^{\alpha}$ for a given irradiation condition such as the irradiation energy or incident angle, $\boldsymbol{\kappa}^I$, and the initial uniform concentration distribution, C^{α_0}, of the substrate. Then, since $dC_i^{\alpha}/dI = 0$ for steady state, the solution of the system of equations, $F_i^{\alpha}\left(\mathbf{C}^{\alpha}; \boldsymbol{\kappa}^I, C^{\alpha_0}\right) = 0, i = 1, \cdots, N$, is the steady-state concentration distribution, $\mathbf{C}^{\alpha} = \mathbf{C}^{\alpha(SS)}\left(\boldsymbol{\kappa}^I, C^0\right)$. The function $F_i^{\alpha}\left(\mathbf{C}^{\alpha}; \boldsymbol{\kappa}^I, C^{\alpha_0}\right)$ is, then, expanded and linearized for $\left|\mathbf{C}^{\alpha} - \mathbf{C}^{\alpha(SS)}\right| \ll 1$ as

$$\frac{dC_i^{\alpha}}{dI} = \sum_{i=k}^{N} X_{ik}^{\alpha}\left(C_k^{\alpha} - C_k^{\alpha(SS)}\right) + O\left(\left|\mathbf{C}^{\alpha} - \mathbf{C}^{\alpha(SS)}\right|^2\right), i = 1, \cdots, N \tag{3}$$

where $X_{ik}^{\alpha} = \partial F_i^{\alpha}/\partial C_k\big|_{\mathbf{C}^{\alpha(SS)}}$ is the inter-layer atom exchange coefficient. X_{ik}^{α} depicts the sputtering process when $i = k$, while it represents the atomic rearrangement process from k to i layer when $i \neq k$. The general solution of the linear kinetic equation is

$$C_i^{\alpha} = C_i^{\alpha(SS)} + \sum_{i=k}^{N} A_k^{\alpha} p_i^k e^{\lambda_k I}, i = 1, \cdots, N \tag{4}$$

where λ_k and p_i^k are the kth eigenvalue and the corresponding eigenvector components of X_{ik}^{α}. The amplitude A_k^{α} is known from the initial concentration distribution $\left(C_i^{\alpha(ini)} = C^{\alpha_0}\right)$ as

$$A_k^{\alpha} = \sum_{i=1}^{N} \left[p^{-1}\right]_i^k \left(C_i^{\alpha(ini)} - C_i^{\alpha(SS)}\right), k = 1, \cdots, N \tag{5}$$

In Fig. 4, we observed that the concentrations of the third and fourth layers do not vary much for both $Co_{0.5}Cu_{0.5}$ alloy and CoAl B2 phase under 0.5 keV Ar bombardment at 300 K. Therefore, we assumed that major rearrangement was made up to $N = 2$, for Eq. (2), to make comparisons between the MD simulations and the kinetic model. Furthermore, we also noticed in $Co_{0.5}Cu_{0.5}$ alloy simulations that the concentration of the second layer decayed monotonically and asymptotically to a steady state value, while that of the first layer approached to another steady state value with one inflection point (see Fig. 4). These observations indicate that R_{21}^{α} in Eq. (3), which represents the net rearrangement of atom $\alpha(=\text{Cu})$ from the first layer to the second layer is negligible for these irradiation conditions. Therefore, for brevity, we assumed that the net sputtering occurred only on the top layer, while the net rearrangement took place from the second layer to the top layer. Composition change in the lower layer than the second one was ignored for simplicity. Sputtering yield and rearrangement yield were assumed constant in this model for the small composition variation $\left(\left|\mathbf{C}^{\alpha} - \mathbf{C}^{\alpha(SS)}\right| \ll 1\right)$. We used the yield values at the initial concentration as the composition-independent yields. Implantation of Ar was not considered since the probability of implantation at low kinetic energy is small; in the present MD simulation, the probabilities were 0.01 for $Co_{0.5}Cu_{0.5}$ alloy and 0.04 for CoAl B2 phase.

Identifying X_{11}^{α} and $X_{12}^{\alpha}\left(=-X_{22}^{\alpha}\right)$ in Eq. (3) with statistical modeling for the MD simulation results as $S_{\alpha}\left(=-Y_{\alpha}^{s}/N_0\right)$ and $R_{\alpha}\left(=Y_{\alpha}^{r}/N_0\right)$ respectively with $N_0 = N_{\alpha} + N_{\beta}$, the total number of atoms in the layer, we have Eq. (3) reduced to

$$\begin{aligned} \frac{dC_1^{\alpha}}{dI} &= -S_{\alpha}C_1^{\alpha} + R_{\alpha}C_2^{\alpha} + Q_1^{\alpha} \\ \frac{dC_2^{\alpha}}{dI} &= -R_{\alpha}C_2^{\alpha} + Q_2^{\alpha} \end{aligned} \tag{6}$$

where $Q_1^{\alpha} = S_{\alpha}C_1^{\alpha(SS)}$ and $Q_2^{\alpha} = R_{\alpha}C_2^{\alpha(SS)}$. Solving Eq. (6) with initial conditions, $C_1^{\alpha}\big|_{I=0} = C_2^{\alpha}\big|_{I=0} = C^{\alpha_0} = 0.5$, gives

$$C_1^{\alpha} = \frac{Q_1^{\alpha}+Q_2^{\alpha}}{S_{\alpha}} + \left\{\frac{Q_2^{\alpha}-C^{\alpha_0}R_{\alpha}}{R_{\alpha}-S_{\alpha}}\right\}\exp\left(-R_{\alpha}I\right) + \left\{C^{\alpha_0} - \frac{(Q_1^{\alpha}+Q_2^{\alpha})R_{\alpha}}{(R_{\alpha}-S_{\alpha})S_{\alpha}} + \frac{Q_1^{\alpha}+C^{\alpha_0}R_{\alpha}}{R_{\alpha}-S_{\alpha}}\right\}\exp\left(-S_{\alpha}I\right) \quad (7)$$

$$C_2^{\alpha} = \frac{Q_2^{\alpha}}{R_{\alpha}} + \left\{C^{\alpha_0} - \frac{Q_2^{\alpha}}{R_{\alpha}}\right\}\exp\left(-R_{\alpha}I\right)$$

The parameters in Eq. (7) were fit with the simulation results as shown in Fig. 4(a) and 4(b), with $\alpha =$ Cu for $Co_{0.5}Cu_{0.5}$ alloy and $\alpha =$ Al for CoAl B2 phase, respectively. Solid lines in Fig. 4 are the best fitting curves of Eq. (7) by using the nonlinear least square Marquardt–Levenberg algorithm. The present kinetic model well-describes the composition modulation behaviors with the *rms* of residuals of 0.66% and 1.29% for the top and the second layer of the $Co_{0.5}Cu_{0.5}$ alloy respectively, and 1.72% and 1.20% for the top and the second layer of the CoAl B2 phase respectively. For the best fitting, we obtained $\frac{R_{Cu}}{S_{Cu}} = \frac{Y_{Cu}^r/N_0}{Y_{Cu}^s/N_0} = \frac{Y_{Cu}^r}{Y_{Cu}^s} = 2.11$ for $Co_{0.5}Cu_{0.5}$ alloy and $\frac{R_{Al}}{S_{Al}} = \frac{Y_{Al}^r/N_0}{Y_{Al}^s/N_0} = \frac{Y_{Al}^r}{Y_{Al}^s} = 6.40$ for CoAl B2 phase. These values are comparable with the yields obtained by the MD simulations (Table 3), $\frac{Y_{Cu}^r}{Y_{Cu}^s} = 1.85$ and $\frac{Y_{Al}^r}{Y_{Cu}^s} = 8.39$. Surprisingly, the only two layer rearrangement model agrees well with the MD simulation results for $Co_{0.5}Cu_{0.5}$ alloys under 0.5 keV Ar bombardment at low temperature (300 K). This analysis supports that the layer-by-layer composition modulation of a binary alloy can be made by ballistic atomic rearrangement near the surface during Ar bombardment even at room temperature. However, some discrepancies exist between the MD simulation results and the two-layer kinetic model in CoAl B2 phase where surface amorphization occurs during the Ar bombardment.

4. Conclusions

The atomic scale MD simulation of Ar bombardments on both a $Co_{0.5}Cu_{0.5}$ random alloy and the CoAl B2-type phase surface at room temperature demonstrated that the layer-by-layer composition modulation occurs on both alloys. The component of higher-sputtering yield accumulates on the topmost surface layer, while it becomes depleted in the secondary layers, which is puzzling in the framework of the conventional sputtering theory. We derived a phenomenological kinetic model based on the MD simulation results considering both the rearrangement and the sputtering of the substrate atoms. The MD results and its kinetic model successfully demonstrated that the rearrangement of the substrate atoms due to ion irradiation plays a significant role in determining the composition modulation. The present work suggests that the rearrangement of surface atom should be properly considered in addition to the sputtering atoms to understand the evolution of surface structure and composition during ion bombardment.

CRediT authorship contribution statement

Byung-Hyun Kim: Conceptualization, Formal analysis, Methodology, Investigation, Writing - original draft, Writing - review & editing. **Sang-Pil Kim:** Conceptualization, Methodology. **Joonhee Kang:** Investigation, Writing - original draft. **Yong-Chae Chung:** Supervision. **Kyung-Suk Kim:** Methodology. **Kwang-Ryeol Lee:** Funding acquisition, Project administration, Supervision, Writing - original draft, Writing - review & editing.

Declaration of Competing Interest

The authors declare that they have no known competing financial interests or personal relationships that could have appeared to influence the work reported in this paper.

Acknowledgments

The present work was supported by the KIST Fundamental Research Program, contract number 2E30460. This research was also funded by the Research and Development Program of Korea Institute of Energy Research (KIER) (C0-2435). Y.-C. C. acknowledges support by the National Research Foundation of Korea (NRF) grant funded by the Korea government (Ministry of Science and ICT) (2019R1A2B5B01070215).

Appendix A. Supplementary material

Supplementary data associated with this article can be found, in the online version, at https://doi.org/10.1016/j.apsusc.2020.148102.

References

[1] F. Tuomisto, I. Makkonen, J. Heikinheimo, F. Granberg, F. Djurabekova, K. Nordlund, G. Velisa, H. Bei, H. Xue, W.J. Weber, Y. Zhang, Segregation of Ni at early stages of radiation damage in NiCoFeCr solid solution alloys, Acta Mater. 196 (2020) 44–51.
[2] E.A. Hodille, J. Byggmästar, E. Safi, K. Nordlund, Sputtering of beryllium oxide by deuterium at various temperatures simulated with molecular dynamics, Phys. Scr. 2020 (2020).
[3] F. Granberg, J. Byggmästar, K. Nordlund, Defect accumulation and evolution during prolonged irradiation of Fe and FeCr alloys, J. Nucl. Mater. 528 (2020).
[4] F. Granberg, A. Litnovsky, K. Nordlund, Low energy sputtering of Mo surfaces, J. Nucl. Mater. 539 (2020) 152274.
[5] F. Djurabekova, C. Fridlund, K. Nordlund, Defect and density evolution under high-fluence ion irradiation of Si/SiO2 heterostructures, Phys. Rev. Mater. 4 (2020) 013601.
[6] E.A. Hodille, J. Byggmastar, E. Safi, K. Nordlund, Molecular dynamics simulation of beryllium oxide irradiated by deuterium ions: Sputtering and reflection, J. Phys. Condens. Matter 31 (2019).
[7] A. Fellman, A.E. Sand, J. Byggmastar, K. Nordlund, Radiation damage in tungsten from cascade overlap with voids and vacancy clusters, J. Phys. Condens. Matter 31 (2019).
[8] K. Jin, W. Guo, C. Lu, M.W. Ullah, Y. Zhang, W.J. Weber, L. Wang, J.D. Poplawsky, H. Bei, Effects of Fe concentration on the ion-irradiation induced defect evolution and hardening in Ni-Fe solid solution alloys, Acta Mater. 121 (2016) 365–373.
[9] F. Granberg, K. Nordlund, M.W. Ullah, K. Jin, C. Lu, H. Bei, L.M. Wang, F. Djurabekova, W.J. Weber, Y. Zhang, Mechanism of Radiation Damage Reduction in Equiatomic Multicomponent Single Phase Alloys, Phys. Rev. Lett. 116 (2016) 135504.
[10] W.L. Chan, E. Chason, Making waves: Kinetic processes controlling surface evolution during low energy ion sputtering, J. Appl. Phys. 101 (2007) 121301.
[11] U. Valbusa, C. Boragno, F.B.D. Mongeot, Nanostructuring surfaces by ion sputtering, J. Phys. Condens. Matter 14 (2002) 8153–8175.
[12] P. Chaudhari, J. Lacey, J. Doyle, E. Galligan, S.C.A. Lien, A. Callegari, G. Hougham, N.D. Lang, P.S. Andry, R. John, K.H. Yang, M.H. Lu, C. Cai, J. Speidell, S. Purushothaman, J. Ritsko, M. Samant, J. Stohr, Y. Nakagawa, Y. Katoh, Y. Saitoh, K. Sakai, H. Satoh, S. Odahara, H. Nakano, J. Nakagaki, Y. Shiota, J. Stöhr, Y. Nakagawa, Y. Katoh, Y. Saitoh, K. Sakai, H. Satoh, S. Odahara, H. Nakano, J. Nakagaki, Y. Shiota, Atomic-beam alignment of inorganic materials for liquid-crystal displays, Nature 411 (2001) 56–59.
[13] S. Facsko, T. Dekorsy, C. Koerdt, C. Trappe, H. Kurz, A. Vogt, H.L. Hartnagel, Formation of Ordered Nanoscale Semiconductor Dots by Ion Sputtering, Science (80-) 285 (1999) 1551–1553.
[14] O. Azzaroni, P.L. Schilardi, R.C. Salvarezza, R. Gago, L. Vázquez, Direct molding of nanopatterned polymeric films: Resolution and errors, Appl. Phys. Lett. 82 (2003) 457–459.
[15] Y.J. Chen, J.P. Wang, E.W. Soo, L. Wu, T.C. Chong, Periodic magnetic nanostructures on self-assembled surfaces by ion beam bombardment, J. Appl. Phys. 91 (2002) 7323–7325.
[16] R. Moroni, D. Sekiba, F. Buatier de Mongeot, G. Gonella, C. Boragno, L. Mattera, U. Valbusa, Uniaxial Magnetic Anisotropy in Nanostructured Co/Cu(001): From Surface Ripples to Nanowires, Phys. Rev. Lett. 91 (2003) 167207.
[17] R.M. Bradley, P.D. Shipman, Spontaneous pattern formation induced by ion bombardment of binary compounds, Phys. Rev. Lett. 105 (2010) 1–4.
[18] P.D. Shipman, R.M. Bradley, Theory of nanoscale pattern formation induced by normal-incidence ion bombardment of binary compounds, Phys. Rev. B - Condens. Matter Mater. Phys. 84 (2011) 1–14.
[19] V.B. Shenoy, W.L. Chan, E. Chason, Compositionally modulated ripples induced by sputtering of alloy surfaces, Phys. Rev. Lett. 98 (2007) 256101.
[20] R.M. Bradley, P.D. Shipman, A surface layer of altered composition can play a key role in nanoscale pattern formation induced by ion bombardment, Appl. Surf. Sci. 258 (2012) 4161–4170.
[21] R.M. Bradley, K.W. Mauser, Can the atomic yields oscillate during ion sputtering of an initially homogeneous multicomponent alloy? J. Appl. Phys. 114 (2013).
[22] F. Reichel, L.P.H. Jeurgens, E.J. Mittemeijer, Modeling compositional changes in binary solid solutions under ion bombardment: Application to the Ar+

bombardment of MgAl alloys, Phys. Rev. B - Condens. Matter Mater. Phys. 73 (2006) 1–11.
[23] P. Sigmund, A mechanism of surface micro-roughening by ion bombardment, J. Mater. Sci. 8 (1973) 1545–1553.
[24] R.M. Bradley, J.M.E. Harper, Theory of ripple topography induced by ion bombardment, J. Vac. Sci. Technol. A Vacuum, Surfaces, Film. 6 (1988) 2390.
[25] N. Lam, Mechanisms and kinetics of ion beam-induced compositional modifications* n. q. lam, Mater. Res. Soc. Symp. Proc. 100 (1988) 29–43.
[26] N. Lam, H. Wiedersich, Bombardment-induced segregation and redistribution, Nucl. Instrum. Methods Phys. Res. Sect. B Beam Interact. with Mater. Atoms 18 (1986) 471–485.
[27] N.Q. Lam, Ion bombardment effects on the near-surface composition during sputter profiling, Surf. Interface Anal. 12 (1988) 65–77.
[28] M. Sckerl, P. Sigmund, N. Lam, Ion-beam induced compositional changes in alloys at elevated temperatures, Nucl. Instrum. Methods Phys. Res. Sect. B Beam Interact. Mater. Atoms 120 (1996) 221–225.
[29] M.W. Sckerl, N.Q. Lam, P. Sigmund, Compositional changes in alloys during ion bombardment at elevated temperatures, Nucl. Instrum. Methods Phys. Res. Sect. B Beam Interact. with Mater. Atoms 140 (1998) 75–90.
[30] H. Gnaser, Low-Energy Ion Irradiation of Solid Surfaces, in: Springer Tracts in Modern Physics, volume 146, Springer Berlin Heidelberg, Berlin, Heidelberg, 1999.
[31] K. Nordlund, Historical review of computer simulation of radiation effects in materials, J. Nucl. Mater. 520 (2019) 273–295.
[32] J. Samela, K. Nordlund, V. Popok, E. Campbell, Origin of complex impact craters on native oxide coated silicon surfaces, Phys. Rev. B 77 (2008) 075309.
[33] J. Samela, K. Nordlund, Atomistic Simulation of the Transition from Atomistic to Macroscopic Cratering, Phys. Rev. Lett. 101 (2008) 027601.
[34] N. Kalyanasundaram, M. Ghazisaeidi, J.B. Freund, H.T. Johnson, Single impact crater functions for ion bombardment of silicon, Appl. Phys. Lett. 92 (2008) 131909.
[35] S.-P. Kim, B.-H. Kim, H. Kim, K.-R. Lee, Y.-C. Chung, J. Seo, J.-S. Kim, Anisotropic rearrangement of the substrate atoms during Ar bombardment on Pd(001) surface, Nucl. Instrum. Methods Phys. Res. Sect. B Beam Interact. with Mater. Atoms 269 (2011) 2605–2609.
[36] G. Guo, H. Wang, Gradient-Corrected Density Functional Calculation of Elastic Constants of Fe, Co and Ni in bcc, fcc and hcp Structures, Chinese J. Phys. 38 (2000), 949–661.
[37] C. Kittel, Introduction to Solid State Physics, Wiley series on the science and technology of materials, Wiley, New York, 1968.
[38] M. Aldén, S. Mirbt, H.L. Skriver, N.M. Rosengaard, B. Johansson, Surface magnetism in iron, cobalt, and nickel, Phys. Rev. B 46 (1992) 6303–6312.
[39] L.Z. Mezey, J. Giber, The Surface Free Energies of Solid Chemical Elements: Calculation from Internal Free Enthalpies of Atomization, Jpn. J. Appl. Phys. 21 (1982) 1569–1571.
[40] P. Villars, Pearson's Handbook: Desk Edition: Crystallographic Data for Intermetallic Phases, ASM International, 1997.
[41] W.F. Gale, T.C. Totemeier, Smithells Metals Reference Book, Elsevier Science, 2003.
[42] R. Hultgren, P.D. Desai, M. Gleiser, D.T. Hawkins, Selected values of the thermodynamic properties of binary alloys, ASM, Ohio, 1973.
[43] S.P. Bafuk, Master's thesis, Michigan Technological University, 1981.
[44] L. Vitos, A.V. Ruban, H.L. Skriver, J. Kollár, The surface energy of metals, Surf. Sci. 411 (1998) 186–202.
[45] X.W. Zhou, R.A. Johnson, H.N.G. Wadley, Misfit-energy-increasing dislocations in vapor-deposited CoFe/NiFe multilayers, Phys. Rev. B - Condens. Matter Mater. Phys. 69 (2004) 144113.
[46] A.F. Voter, S.P. Chen, Accurate Interatomic Potentials for Ni, Al and Ni3Al, Mater. Res. Soc. Symp. Proc. 82 (1987) 175–180.
[47] R. Pasianot, E.J. Savino, Embedded-atom-method interatomic potentials for hcp metals, Phys. Rev. B 45 (1992) 12704–12710.
[48] C. Vailhe, D. Farkas, Shear faults and dislocation core structure simulations in B2 FeAl, J. Mater. Res. 12 (1997) 2559.
[49] J.F. Ziegler, J.P. Biersack, U. Littmark, The Stopping and Range of Ions in Solids, Stopping and ranges of ions in matter, Pergamon, 1985.
[50] S. Plimpton, Fast parallel algorithms for short-range molecular dynamics, J. Comput. Phys. 117 (1995) 1–19.
[51] E. Bringa, K. Nordlund, J. Keinonen, Cratering-energy regimes: From linear collision cascades to heat spikes to macroscopic impacts, Phys. Rev. B 64 (2001) 235426.
[52] V. Blum, C. Rath, G.R. Castro, M. Kottcke, L. Hammer, K. Heinz, Ordered and Disordered Rippling in the CoAl(110)-(1×1) Surface, Surf. Rev. Lett. 03 (1996) 1409–1415.